


Efficient Transport Between Disjoint Nanochannels by a Water Bridge

Muhammad Sahimi^{1,*} and Fatemeh Ebrahimi^{2,†}

¹*Mork Family Department of Chemical Engineering and Materials Science, University of Southern California, Los Angeles, California 90089-1211, USA*

²*Department of Physics, University of Birjand, Birjand 97175-615, Iran*

 (Received 16 January 2019; revised manuscript received 6 April 2019; published 31 May 2019)

Water channels are important to new purification systems, osmotic power harvesting in salinity gradients, hydroelectric voltage conversion, signal transmission, drug delivery, and many other applications. To be effective, water channels must have structures more complex than a single tube. One way of building such structures is through a *water bridge* between two disjoint channels that are not physically connected. We report on the results of extensive molecular dynamics simulation of water transport through such bridges between two carbon nanotubes separated by a nanogap. We show that not only can pressurized water be transported across a stable bridge, but also that (i) for a range of the gap's width l_g the bridge's hydraulic conductance G_b does not depend on l_g , (ii) the overall shape of the bridge is not cylindrical, and (iii) the dependence of G_b on the angle between the axes of two nonaligned nanochannels may be used to tune the flow rate between the two.

DOI: 10.1103/PhysRevLett.122.214506

Fabrication of water channels and understanding the dynamics of flow in them have attracted wide attention. The problem was originally motivated by the need for new purification systems [1,2] for drinking water as large parts of Earth is afflicted by prolonged draught. Man-made channels for water transport have numerous other applications, including osmotic power harvesting in salinity gradients [3] and hydroelectric voltage conversion [4], conversion and multiplications by polar molecules [5,6], advanced conductance systems such as water channel proteins [7], and releasing biomolecules during drug delivery [8]. Carbon [9], boron nitride [10], and graphene oxide nanotubes [11] have been used as the building blocks of such channels. To be effective, artificial water channels must have more complex structures than a single tube. For example, many purification processes are based on multiple channels with a variety of sizes. Although microfluidic systems with a Y shape (a tube branching into two others) [12] and nanofluidic systems that consist of nanotubes of various sizes connected together by nanojunctions [13] have been proposed, it is still very difficult to fabricate complex structures with interconnected nanotubes.

One possibility is water bridges, i.e., those made of water between two channels separated by some distance. Such bridges have been set up experimentally between two beakers [14,15], and by an atomic-resolution force microscope [16]. In this Letter we report on the results of an extensive study of the properties of bridges between two single-wall carbon nanotubes (CNTs) for efficient transport of water across the nanogap between the two CNTs. We demonstrate that, for an optimal pressure difference and

gap width, the bridge is capable of supporting stable water flow between the two CNTs. To our knowledge, our study represents the first of its kind.

We used molecular dynamics (MD) simulation to study the problem. The system consists of two water reservoirs separated by a distance $L = 74 \text{ \AA}$ along the nanotubes' axes in the z direction, each consisting of two parallel graphene sheets normal to the z axis; see Fig. 1. At time $t = 0$ the distance between the two sheets in each reservoir was 81.4 \AA , each filled by 16 848 water molecules and distributed on a simple-cubic lattice. Two identical and coaxial (12,12) CNTs with radius 6.5 \AA and separated by a gap of length l_g were connected to the reservoirs. The entrance to the left CNT represents $z = 0$, while the exit of the right CNT is at $z = L$ with the nanotubes' length being H . The outermost graphene sheet in each reservoir acted as a piston exerting constant pressures P_l on the left and $P_r < P_l$ on the right. Periodic boundary conditions were imposed in the transverse directions.

Water molecules were represented by the TIP3P model, and their interactions with the carbon atoms were represented by the Lennard-Jones potential with the usual energy and size parameters ϵ and σ , calculated on the basis of the interactions between the water oxygen and the carbon atoms. To study the effect of the interaction parameters and the contact angle θ between the water droplets and the carbon surface, we used two force fields (FF). One was the AMBER96 FF [17] for which, $\epsilon_{O-C} = 0.4784 \text{ kJ/mol}$ and $\sigma_{O-C} = 3.28 \text{ \AA}$ that correspond to $\theta \approx 57^\circ$ [18]. For the second FF [19], $\epsilon_{O-C} = 0.392 \text{ kJ/mol}$ and $\sigma_{O-C} = 3.19 \text{ \AA}$, corresponding to $\theta \approx 86^\circ$. The two sets of

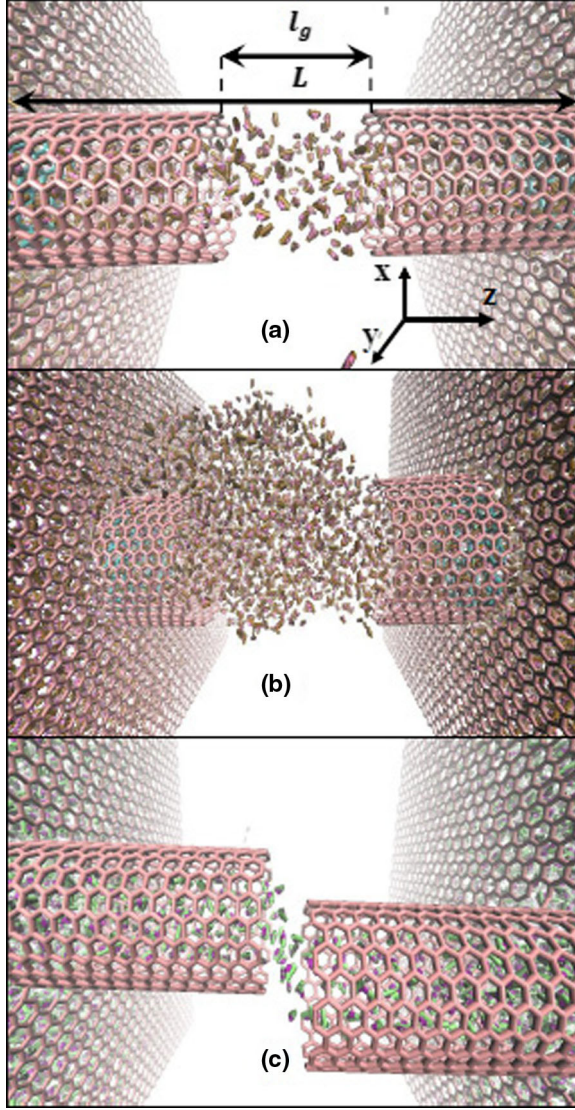


FIG. 1. (a) A stable bridge. (b) Only part of the pressurized water is transported across the gap. (c) Stable bridge between two nonaligned nanochannels.

parameters correspond to hydrophilic and hydrophobic CNT surface, respectively. We used a cutoff distance of 1.4 nm for the extent of the Lennard-Jones interactions. The particle-particle-particle-mesh method was used to compute the long-range Coulombic interactions.

Initially, the simulations were carried out in the NVT ensemble at $T = 300$ K using the LAMMPS package [20] with a time step of 2 fs. The density of water at 300 K is 0.98 g/cm³. Both CNTs were initially capped. The water-reservoir system reached equilibrium after typically 0.2 ns, after which the caps were removed to allow water to enter the CNTs. Then, the thermostat was also removed and the simulations were continued in the NVE ensemble. In the NVE ensemble the temperature T can rise due to dissipation of mechanical energy whose main source is the applied pressure (see also below). We should note,

however, that once water enters the right CNT, mechanical energy is needed to move the piston in the right reservoir to create the required space for the arriving water molecules. As a result, the dissipated energy is very small and the simulations indicated that T increases by at most 5 K. We mostly used the pressures $P_l = 1001$ and $P_r = 1$ atm, and varied the gap length l_g up to 40 Å to estimate Q , the volume flow rate of water passing through. For comparison, we also carried out simulations for $l_g = 0$, i.e., a single pristine CNT. For the hydrophobic case the upstream pressure P_l must be large; otherwise, water will have great difficulty entering the CNT on the left side. The Reynolds number of the flow was about 0.3. Duration of each simulation run was 2 ns. Longer preliminary simulations did not produce results distinctly different from what we present below.

Flow of water in small nanotubes does not satisfy the no-slip boundary condition. Moreover, in small constrictions and for strong wall-fluid interactions, the positions of the fluid molecules are strongly correlated with perfect spatial ordering [21–23], which may affect fluid flow. Previous MD simulations indicated, however, that water flow in (12,12) CNTs (and similar small CNTs) has the characteristics of bulk flow for both hydrophobic [21] and hydrophilic [24] interactions, and that the steady-state condition is described [18,25,26] by a modified Hagen-Poiseuille equation that takes into account both the access resistance Ω_a due to the entrance losses and the hydraulic resistance Ω_i within the CNTs. Thus, if, $Q = \Delta P / \Omega$, with $\Omega = \Omega_a + \Omega_i$, we have, $\Omega_a = \eta C / R^3$ with η being the dynamic viscosity of water, and C a numerical constant ≈ 3 , and $\Omega_i = 8\eta H / [\pi(R^4 + 4R^3b)]$, where b is the slip length.

Capillary forces play the most important role in the first stage of filling the CNTs. Over a period of less than 0.1 ns the number of water molecules in both reservoirs reduces, as they begin filling the CNTs. In a nanocapillary the volume flow rate Q that penetrates the nanotubes and the reservoir pressure P are related by [27–29]

$$P - P_0 = \frac{\eta C' Q}{R^3} + \frac{8\eta Q h(t)}{\pi(R^4 + 4R^3b)} - \frac{2\gamma \cos \theta}{R}, \quad (1)$$

where P_0 is the ambient pressure, $C' = C/2$, and $h(t)$ is the temporal location of the contact line from the entrance inside the tube. In the case of hydrophobic surfaces, a minimum pressure, $P_{\min} = -2\gamma \cos \theta / R$, is needed for water to penetrate the nanotube, i.e., $P_{\min} \approx 190$ atm. Note that with the hydrophobic CNTs water still penetrates the right CNT from the low-pressure reservoir on the right side by slow diffusion [30].

After filling the left CNT, water leaves it and enters the space between the two CNTs, forming a drop at its mouth. The maximum pressure $P(R)$ that can be applied to the flow without detaching the drop is the Laplace pressure, $P(R) - P_0 = 2\gamma / R$ [31]. With $R = 6.5$ Å, $\gamma = 0.072$ N/m,

and $P_0 \approx 0$, we obtain $P \approx 2000$ atm, twice P_l in the simulations. The assumption that $P_0 \approx 0$ is not really accurate though, because when the right CNT is filled by water, the affinity of water molecules for each other generates a negative pressure just outside its entrance. In addition, with hydrophilic carbon walls, the attractive forces exerted by the walls' atoms on the water molecules should also be taken into account. This explains why the growing water nanodrops at the left CNT's exit eventually form a stable bridge to the right CNT, even at a pressure of $P_l = 1000$ atm. For large gap width, water still leaves the highly pressurized side, but its flow is unstable, and a portion of it cannot reach the right CNT.

The simulations indicate that if P_l in the left reservoir is high enough, then, depending on the system's conditions, three types of flow may develop: (i) a stable nanobridge that transports almost all the water from the CNTs on the left toward the one across the gap; (ii) a jetlike unstable flow from the CNT on the left that, instead of moving toward the one on the right, accumulates on and near the sheet on the left; and (iii) a flow system in which only a part of the pressurized water is transported to the right CNT via a water bridge, with the rest released similar to a nanojet into the free space. These are shown in Fig. 1. If P_l is not high enough, then a pendant drop of water forms at the left CNT' exit, but does not detach itself from the nanotube.

In case (i) a continuous and stable bridge is formed across the gap, if the gap width l_g does not exceed a certain threshold. For example, with both hydrophilic and hydrophobic carbon walls and $P_l = 1000$ atm, water flow between the two CNTs is maintained for ≤ 25 Å, which is comparable with the maximum length of 24 Å for a water bridge formed by capillary affinity, one in which water is transported only by diffusion. At higher pressures, however, say $P_l = 1500$ atm, which is still significantly less than the threshold value set by Eq. (1), flow instabilities develop in the water flow across the gap [see Fig. 1(a)], which is the type of instability that results in the formation of the nanojet [see Fig. 1(b)] that has been already studied [32–35].

Figure 2 presents the dependence of the temporal variations of the number of water molecules, which leave the high-pressure reservoir, on the gap width and the type of wall-water interactions. Three stages of water transport is identified in each case: (i) penetrating the CNT on the left whose early stage of filling the nanotube is dominated by capillary forces, (ii) forming pressurized water drops at the exit of the left CNT (the flat part in Fig. 2) that may take a relatively long time for large gaps and hydrophobic interaction, and (iii) forming a stable water bridge between the two CNTs. These are all consistent with our discussions above.

We calculated the water volume flow rate $Q = (m/\rho)\Delta N/\Delta t$ at steady state that leaves the left CNT and enters the right nanotube, with ρ and m being the

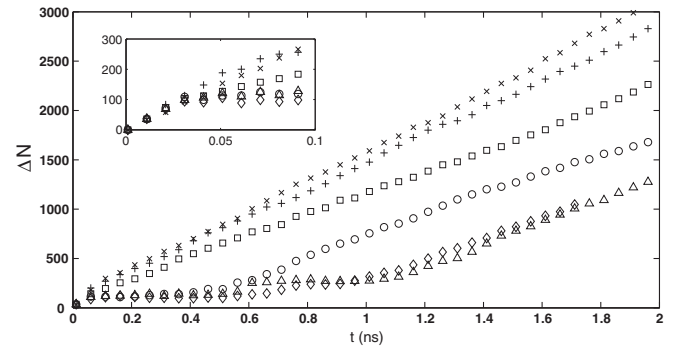


FIG. 2. Temporal variation of the decrease ΔN of the number of water molecules N in the high-pressure reservoir for gap width $l_g = 0.0$ and hydrophobic CNT (+) and hydrophilic CNT (\times); $l_g = 9.8$ Å and hydrophobic CNT (square); $l_g = 14.8$ Å and hydrophobic CNT (triangle); $l_g = 24.6$ Å and hydrophilic CNT (circle), and $l_g = 34.4$ Å and hydrophilic CNT (diamond). The inset shows the early time behavior.

density and mass of the water, and studied its dependence on l_p . The results for hydrophilic walls are depicted in Fig. 3, indicating that for $l_g < 25$ Å all the water that leaves the left CNT enters the right one, except perhaps for a few molecules that evaporate in the gap. The same behavior develops for the hydrophobic interaction, hence demonstrating that the bridge is viable. For 25 Å $< l_g < 35$ Å water still flows across the gap, but its flow rate is neither steady nor equal in both CNTs; i.e., not all the water exiting the left CNT reaches the right one.

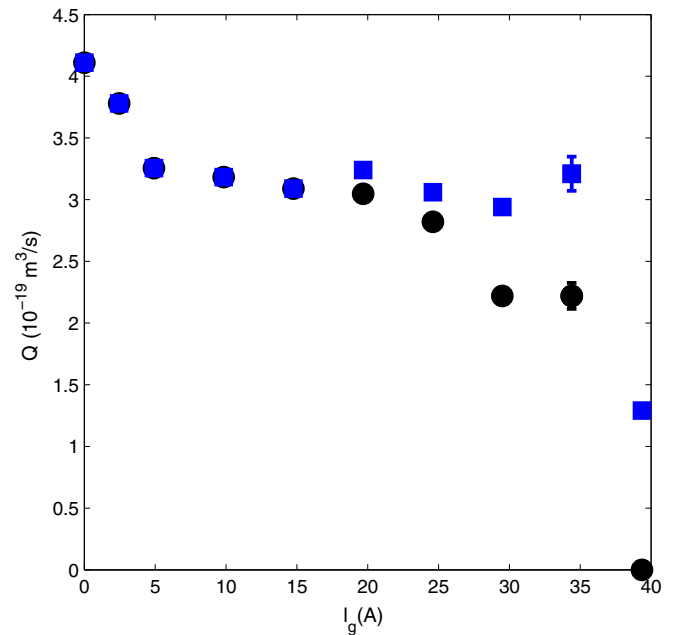


FIG. 3. Dependence of water volume flow rate Q on the gap's width l_g for hydrophilic CNTs in the left (circles) and the right reservoir (squares) in a stable bridge. Note the equality of Q in the two nanotubes.

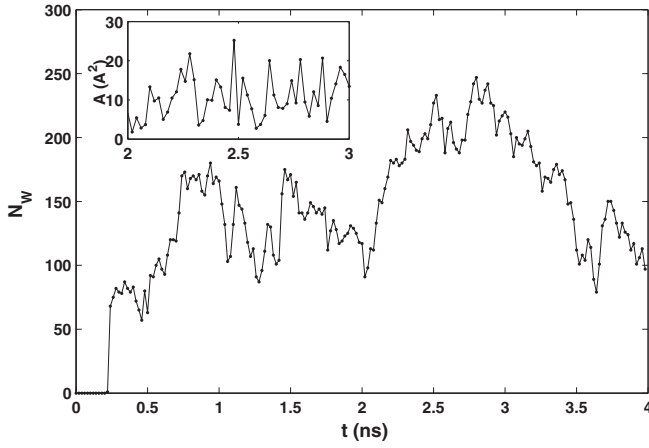


FIG. 4. Temporal fluctuation of the number of water molecules in the bridge for a gap of width 19.7 Å. The inset shows the acylindricity A of the bridge.

Properties of the water bridge.—Both the instantaneous and time-averaged properties of the water bridge manifest important features. Figure 3 indicates that, after an initial steep decrease in the bridge’s hydraulic conductance Ω over a length that is at most twice the size of the water molecule; Ω is essentially constant over a relatively wide interval of the gap width, [5 Å, 25 Å], for both hydrophilic and hydrophobic CNTs. Beyond the plateau, the flow rate arriving in the right CNT begins to decrease rapidly. It eventually vanishes, as the bridge is unsustainable when the gap is large. But before that happens, instability develops in the fluid flow on both sides of the gap. For $l_g > 35$ Å, water flow coming out of the left CNT exhibits jetlike behavior; see Fig. 1(b).

A quantitative measure of the shape of a cluster that consists of N_w particles is the eigenvalues of its gyration tensor, $\mathbf{G} = (1/N_w) \sum_{i=1}^{N_w} (\mathbf{X}_i^2 \mathbf{I} - \mathbf{X}_i \mathbf{X}_i)$, with \mathbf{X}_i being the distance of the i th water molecule from the cluster’s center of mass, and \mathbf{I} the unit tensor. We used an efficient method [36] to determine the eigenvalues of \mathbf{G} , namely, λ_x^2 , λ_y^2 , and λ_z^2 , the *acylindricity* of the bridge, $A = |\langle \lambda_x^2 \rangle - \langle \lambda_y^2 \rangle|$, and the mean transverse radius of gyration, $R_g^2 = \frac{1}{2} (\langle \lambda_x^2 \rangle + \langle \lambda_y^2 \rangle)$. They vary rapidly as the water clusters evolve during the simulation. The evolution of N_w and A for a gap of width $l_g \approx 20$ Å and hydrophilic walls are depicted in Fig. 4. We estimate that $R_g = 4.7 \pm 2.8$ Å, $A = 10 \pm 6$ Å², and $N_w = 150 \pm 50$, with the error bars representing the fluctuations over time. For $l_g = 0$ (a single CNT) we obtain $A = 8.4 \pm 0.8$ Å². These are typical values for all the cases that we studied and indicate that (i) the *overall* shape of the water bridge is neither necessarily cylindrical, nor constant in time, and (ii) the cross section of the bridge is larger than the diameter of the CNTs, hence indicating expansion and contraction of the streamlines at the high- and low-pressurized sides,

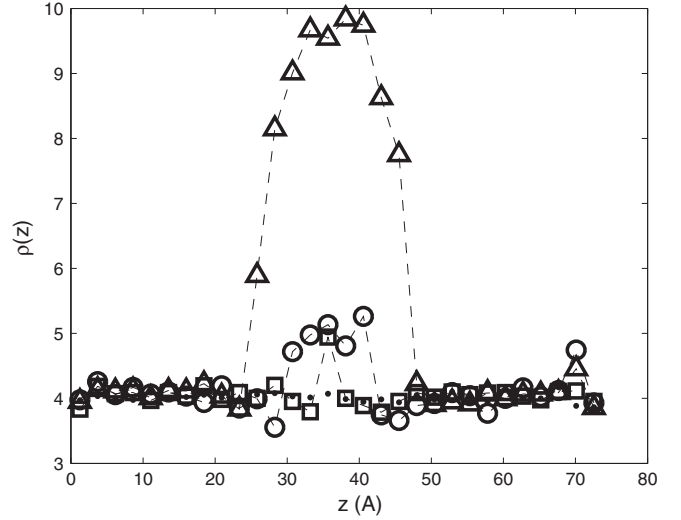


FIG. 5. Time-averaged axial density $\rho(z)$ of the water molecules along the transport path for the gap widths $l_g = 0.0$ Å (dots), 4.9 Å (squares), 14.7 Å (circles), and 19.7 Å (hats) with hydrophilic nanotubes.

respectively. The expansion and contraction generate large fluid velocity gradient, $\nabla \mathbf{v}$, resulting in a viscous dissipation rate [13], $\eta \Phi = -(\boldsymbol{\tau} : \nabla \mathbf{v})$, with $\boldsymbol{\tau}$ being the stress tensor. This explains how the gap induces additional hydraulic resistance in the bridge.

Having demonstrated the effect of viscous dissipation in the bridge, we inspect the plateau region in Fig. 3. The axial density of water, $\rho(z) = (1/\Delta z) \langle N_w(z, z + \Delta z) \rangle$ in the gap, where $\langle \cdot \rangle$ represents an average over the duration of the simulation, providing insight into the bridge’s conductance. The results for four gap widths l_g and hydrophilic walls are shown in Fig. 5, indicating that for $l_g > 5$ Å the mean axial density, in addition to expansion (contraction) area of the streamlines near the high (low) pressurized CNT, has an essentially parabolic shape centered in the middle of the gap in which the $\nabla_z \rho(z)$ is relatively small. Therefore, on average, the middle part of the bridge may be regarded as roughly cylindrical whose length increases as l_g does. Since at steady state the mass of water in this region is constant, the radius of the cylindrical area in the middle must also increase with l_g . This implies that for steady-state flow in the bridge the hydraulic resistance of this region is much smaller than when $l_g = 0$. Thus, the plateau region of Fig. 3 is due to the reduction in the hydraulic resistance in the middle part of the gap that offsets the increase in the resistance arising from viscous dissipation due to the deformation of the streamlines next to the CNTs’ opening.

To test this we carried out MD simulations with two nonaligned CNTs by displacing the center of the right CNT’s entrance by $\Delta x = \Delta y = \Delta z = 5$ Å. Then, the gap’s width, defined as the center-to-center distance between the two CNTs is $l_g = 8.6$ Å. A snapshot of the configuration is shown in Fig. 1(c). The rate of water transport across the

slanted bridge, $dN/dt \approx 700 \pm 20$ (water molecules/ns), is about 50 percent of that of the pristine CNT ($l_g = 0$) and 70 percent of its value in the plateau region for the aligned CNTs. Such a remarkable reduction in hydraulic conductance is due to convergence and divergence of the streamlines around the CNTs' openings into the gap, with additional curvature imposed by the nonaligned geometry, and the reduction of the effective cross section of fluid flow.

Summarizing, with proper design and conditioning, water can be transported efficiently via a bridge across nanoscale gaps between two disjoint nanochannels, such as CNTs. For a range of the gap's width, the hydraulic conductance of the bridge is essentially constant, supporting a stable bridge. The overall shape of the bridge is not cylindrical. The hydraulic conductance of a curved bridge between two nonaligned nanotubes changes rapidly with the tilt angle between the two CNTs, which can be exploited in practice for tuning the flow rate in nanofluidic devices, such as nanovalves. These features should find applications in the development of new types of nanomembranes with separable parts, as well as designing new nanofluidic devices and circuitry. Since the formation of a nano-water bridge depends on the existence of a water column in both nanochannels, the system can be used as a water sensor, or as a one-way path (diode) for fluid transport.

We thank G.R. Maktabdaran for his help. All the simulations were carried using the Saffron computer cluster at the University of Birjand, Iran.

*moe@usc.edu

†f_brahim@birjand.ac.ir

- [1] M. A. Shannon, P. W. Bohn, M. Elimelech, J. G. Georgiadis, B. J. Marinas, and A. M. Mayes, Science and technology for water purification in the coming decades, *Nature (London)* **452**, 301 (2008).
- [2] H. Y. Yang, Z. J. Han, S. F. Yu, K. L. Pey, K. Ostrikov, and R. Karnik, Carbon nanotube membranes with ultrahigh specific adsorption capacity for water desalination and purification, *Nat. Commun.* **4**, 2220 (2013).
- [3] A. Siria, P. Poncharal, A.-L. Biance, R. Fulcrand, X. Blase, S. T. Purcell, and L. Bocquet, Giant osmotic energy conversion measured in a single transmembrane boron nitride nanotube, *Nature (London)* **494**, 455 (2013).
- [4] Q. Yuan and Y.-P. Zhao, Hydroelectric voltage generation based on water-filled single-walled carbon nanotubes, *J. Am. Chem. Soc.* **131**, 6374 (2009).
- [5] Y. Tu, P. Xiu, R. Wan, J. Hu, R. Zhou, and H. Fang, Water-mediated signal multiplication with Y-shaped carbon nanotubes, *Proc. Natl. Acad. Sci. U.S.A.* **106**, 18120 (2009).
- [6] Y. Tu, R. Zhou, and H. Fang, Signal transmission, conversion and multiplication by polar molecules confined in nanochannels, *Nanoscale* **2**, 1976 (2010).
- [7] B. Liu, X. Li, B. Li, B. Xu, and Y. Zhao, Carbon nanotube based artificial water channel protein: Membrane perturbation and water transportation, *Nano Lett.* **9**, 1386 (2009).
- [8] P. Xiu, B. Zhou, W. Qi, H. Lu, Y. Tu, and H. Fang, Manipulating biomolecules with aqueous liquids confined within single-walled nanotubes, *J. Am. Chem. Soc.* **131**, 2840 (2009).
- [9] G. Zuo, R. Shen, S. Ma, and W. Guo, Transport properties of single-file water molecules inside a carbon nanotube biomimicking water channel, *ACS Nano* **4**, 205 (2010).
- [10] G. Tocci, L. Joly, and A. Michaelides, Friction of water on graphene and hexagonal boron nitride from *ab initio* methods: Very different slippage despite very similar interface structures, *Nano Lett.* **14**, 6872 (2014).
- [11] R. R. Nair, H. A. Wu, P. N. Jayaram, I. V. Grigorieva, and A. K. Geim, Unimpeded permeation of water through helium-leak-tight graphene-based membranes, *Science* **335**, 442 (2012).
- [12] L. Liu and X. Chen, Nanofluidic transport in branching nanochannels: A molecular sieve based on Y-junction nanotubes, *J. Phys. Chem. B* **113**, 6468 (2009).
- [13] F. Ebrahimi, F. Ramazani, and M. Sahimi, Nanojunction effects on water flow in carbon nanotubes, *Sci. Rep.* **8**, 7752 (2018).
- [14] E. C. Fuchs, J. Woisetschläger, K. Gatterer, E. Maier, R. Pecnik, G. Holler, and H. Eisenkölb, The floating water bridge, *J. Phys. D* **40**, 6112 (2007).
- [15] R. M. Namin, S. A. Lindi, A. Amjadi, N. Jafari, and P. Irajizad, Experimental investigation of the stability of the floating water bridge, *Phys. Rev. E* **88**, 033019 (2013).
- [16] H. Choe, M. H. Hong, Y. Seo, K. Lee, G. Kim, Y. Cho, J. Ihm, and W. Jhe, Formation, Manipulation, and Elasticity Measurement of a Nanometric Column of Water Molecules, *Phys. Rev. Lett.* **95**, 187801 (2005).
- [17] G. Hummer, J. C. Rasaiah, and J. P. Noworyta, Water conduction through the hydrophobic channel of a carbon nanotube, *Nature (London)* **414**, 188 (2001).
- [18] L. Joly, Capillary filling with giant liquid/solid slip: Dynamics of water uptake by carbon nanotubes, *J. Chem. Phys.* **135**, 214705 (2011).
- [19] T. Werder, J. Walther, R. L. Jaffe, T. Halicioglu, and P. Koumoutsalos, On the water-carbon interaction for use in molecular dynamics simulations of graphite and carbon nanotubes, *J. Phys. Chem. B* **107**, 1345 (2003).
- [20] https://lammps.sandia.gov/doc/Packages_user.html.
- [21] J. A. Thomas and A. J. H. McGaughey, Water Flow in Carbon Nanotubes: Transition to Subcontinuum Transport, *Phys. Rev. Lett.* **102**, 184502 (2009).
- [22] H. Abtahinia and F. Ebrahimi, Monte Carlo study of structural ordering of Lennard-Jones fluids confined in nanochannels, *J. Chem. Phys.* **133**, 064502 (2010).
- [23] M. Khademi and M. Sahimi, Molecular dynamics simulation of pressure-driven water flow in silicon-carbide nanotubes, *J. Chem. Phys.* **135**, 204509 (2011).
- [24] F. Ramazani and F. Ebrahimi, Water imbibition into non-polar nanotubes with extended topological defects, *Chem. Phys.* **476**, 23 (2016).

- [25] S. Gravelle, L. Joly, C. Ybert, and L. Bocquet, Large permeabilities of hourglass nanopores: From hydrodynamics to single file transport, *J. Chem. Phys.* **141**, 18C526 (2014).
- [26] T. B. Sisan and S. Lichter, The end of nanochannels, *Microfluid. Nanofluid.* **11**, 787 (2011).
- [27] J. H. Walther, K. Ritos, E. R. Cruz-Chu, C. M. Megaridis, and P. Koumoutsakos, Barriers to superfast water transport in carbon nanotube membranes, *Nano Lett.* **13**, 1910 (2013).
- [28] R. Lucas, Ueber das zeitgesetz des kapillaren aufstiegs von flüssigkeiten, *Kolloid Z.* **23**, 15 (1918).
- [29] E. W. Washburn, The dynamics of capillary flow, *Phys. Rev.* **17**, 273 (1921).
- [30] A. Striolo, The mechanism of water diffusion in narrow carbon nanotubes, *Nano Lett.* **6**, 633 (2006).
- [31] E. Y. Bormashenko, *Wetting of Real Surfaces* (De Gruyter, Berlin, 2013), p. 40.
- [32] M. Moseler and U. Landman, Formation, stability, and breakup of nanojets, *Science* **289**, 1165 (2000).
- [33] Y. S. Choi, S. J. Kim, and M.-U. Kim, Molecular dynamics of unstable motions and capillary instability in liquid nanojets, *Phys. Rev. E* **73**, 016309 (2006).
- [34] I. Hanasaki and A. Nakatani, Water flow through carbon nanotube junctions as molecular convergent nozzles, *Nanotechnology* **17**, 2794 (2006).
- [35] I. Hanasaki, T. Yonebayashi, and S. Kawano, Molecular dynamics of a water jet from a carbon nanotube, *Phys. Rev. E* **79**, 046307 (2009).
- [36] J. Kopp, Efficient numerical diagonalization of Hermitian 3×3 matrices, *Int. J. Mod. Phys. C* **19**, 523 (2008).